JHEP

Published for SISSA by Springer

Received: December 17, 2018
Revised: May 10, 2019
Accepted: June 27, 2019
Published: July 10, 2019

Exploring inert scalars at CLIC

Jan Kalinowski,[a] **Wojciech Kotlarski,**[b] **Tania Robens,**[c,d] **Dorota Sokołowska**[a,e] **and Aleksander Filip Żarnecki**[a]

[a] *Faculty of Physics, University of Warsaw, Pasteura 5, 02-093 Warszawa, Poland*
[b] *Institut für Kern- und Teilchenphysik, TU Dresden, Dresden, Germany*
[c] *MTA-DE Particle Physics Research Group, University of Debrecen, Poroszlay ut, Debrecen, Hungary*
[d] *Theoretical Physics Division, Rudjer Boskovic Institute, Bijenicka cesta, Zagreb, Croatia*
[e] *International Institute of Physics, Universidade Federal do Rio Grande do Norte, Campus Universitario, Lagoa Nova, Natal-RN 59078-970, Brazil*

E-mail: jan.kalinowski@fuw.edu.pl, wojciech.kotlarski@tu-dresden.de, trobens@irb.hr, dsokolowska@iip.ufrn.br, filip.zarnecki@fuw.edu.pl

Abstract: We investigate the prospect of discovering the Inert Doublet Model scalars at CLIC. As signal processes, we consider the pair-production of inert scalars, namely $e^+e^- \to H^+H^-$ and $e^+e^- \to AH$, followed by decays of charged scalars $H^\pm$ and neutral scalars A into leptonic final states and missing transverse energy.

We focus on signal signatures with two muons or an electron and a muon pair in the final state. A number of selected benchmark scenarios that cover the range of possible collider signatures of the IDM are considered. For the suppression of SM background with the same visible signature, multivariate analysis methods are employed. For several benchmark points discovery is already possible at the low-energy stage of CLIC. Prospects of investigating scenarios that are only accessible at higher collider energies are also discussed.

Keywords: Beyond Standard Model, Higgs Physics

ArXiv ePrint: 1811.06952

https://doi.org/10.1007/JHEP07(2019)053

JHEP07(2019)053

Contents

JHEP07(2019)053

1 Introduction

A number of astrophysical observations based on gravitational interactions point to the existence of dark matter (DM) in the Universe, which can not be described with the Standard Model (SM). One of the simplest extensions of the SM, which can provide a dark matter candidate is the Inert Doublet Model (IDM) [1–3]. The scalar sector of the IDM consists of two SU(2) doublets where one is the SM-like Higgs doublet, Φ_S, while the other is called inert or dark doublet, Φ_D. After electroweak symmetry breaking the sector has five physical states: apart from the SM Higgs boson h it has two neutral ones, H and A, as well as two charged scalars, $H^\pm$. A discrete Z_2 symmetry prohibits the inert scalars from interacting with the SM fermions through Yukawa-type interactions and makes the lightest neutral scalar, chosen to be H in this work, a good dark matter candidate.

In this work we study the potential of CLIC running at three energy stages as a discovery machine for the IDM scalars. We consider neutral scalar (HA) and charged scalar (H^+H^-) pair-production at center-of-mass energies of 380 GeV, 1.5 TeV and 3 TeV. We explore a set of benchmark points (BPs) proposed in [4], which satisfy all the recent experimental and theoretical constraints, provide the neutral H boson as the dark matter candidate ($m_H < m_{H^\pm}, m_A$), and span the inert scalar mass range from about 50 GeV to 1 TeV. Earlier analyses of the IDM at colliders were done in [2, 5–30].

The paper is organized as follows. The structure of the IDM scalar sector and the considered benchmark points are briefly described in section 2. In section 3 the analysis strategy and simulation tools are described. In section 4 results on the possible measurement of low-mass benchmark points at the first stage of CLIC, at 380 GeV, are presented, while section 5 discusses the prospects for heavy inert scalar production at high-energy CLIC. Finally, the conclusions are given in section 6.

2 Inert Doublet Model

The scalar sector of the IDM consists of two scalar doublets, the SM Higgs doublet Φ_S with SM-like Higgs boson h and the inert doublet Φ_D with four inert scalars H, A, $H^\pm$. A discrete Z_2 symmetry is imposed under which the SM-like Higgs doublet Φ_S and all the other SM fields are *even*, whereas the inert doublet Φ_D is *odd*. As a result, inert scalars do not interact with the SM fermions through Yukawa-type interactions, and the most general renormalizable scalar potential for the IDM is given by

$$\begin{aligned} V = &-\frac{1}{2}\left[m_{11}^2(\Phi_S^\dagger\Phi_S)+m_{22}^2(\Phi_D^\dagger\Phi_D)\right] + \frac{\lambda_1}{2}(\Phi_S^\dagger\Phi_S)^2+\frac{\lambda_2}{2}(\Phi_D^\dagger\Phi_D)^2 \\ &+\lambda_3(\Phi_S^\dagger\Phi_S)(\Phi_D^\dagger\Phi_D)+\lambda_4(\Phi_S^\dagger\Phi_D)(\Phi_D^\dagger\Phi_S) + \frac{\lambda_5}{2}\left[(\Phi_S^\dagger\Phi_D)^2+(\Phi_D^\dagger\Phi_S)^2\right]. \end{aligned} \tag{2.1}$$

A more detailed discussion of the potential and physical parameters can be found in section 2 of [23].

Due to the exact Z_2 symmetry, the lightest neutral scalar H (or A) is stable and thereby may serve as a good dark matter candidate. In this work we choose H to be the lightest particle (choosing A instead of H as the lightest particle changes only the meaning of $\lambda_5 \to -\lambda_5$). After fixing the SM-like Higgs boson mass to $m_h = 125.1\,\text{GeV}$ and the vacuum expectation value of the SM-like doublet to $v = 246\,\text{GeV}$ (the SM value) we are left with 5 free parameters, which we take as

$$m_H, m_A, m_{H^\pm}, \lambda_2, \lambda_{345}, \tag{2.2}$$

where $\lambda_{345} = \lambda_3 + \lambda_4 + \lambda_5$ determines the Higgs-DM coupling, while λ_2 corresponds to couplings within the dark sector.

To study the prospects of IDM scalar measurement at CLIC we consider a set of benchmark points proposed in [4], and listed in table 1 for the low-mass benchmarks accessible at 380 GeV, and in table 2 for the high-mass benchmarks accessible only at higher collider energies of 1.5 and 3 TeV. These benchmarks were selected from a larger set of points in the IDM parameter space, which were found to be in agreement with all the theoretical and current experimental constraints. Points corresponding to different assignment of masses and couplings were selected in the parameter range interesting in view of future linear e^+e^- collider searches.

We refer the reader to [4, 23, 29] for a detailed discussion of the theoretical and experimental constraints and the benchmark selection; comments on the impact of future XENON-nT measurements and prospects of testing the IDM model at the LHC can be found in [4]. We summarize the crucial points of the discussion presented there below.

Theoretical and experimental constraints. As theoretical constraints, positivity of the potential [31], the condition to be in the global inert vacuum [32] and perturbative unitarity [33, 34] have been imposed. We also require agreement with electroweak precision tests [35] via oblique parameters [36–39], zero contributions to electroweak gauge boson widths from inert particles by kinematically forbidding decays $W^\pm \to AH^\pm, HH^\pm, Z \to AH, H^+H^-$ [40], and agreement with recasts of LEP and LHC searches [6, 20], including a

JHEP07(2019)053

No.	m_H	m_A	$m_{H^\pm}$	λ_2	λ_{345}	$\Omega_c h^2$
BP1	72.77	107.8	114.6	1.445	-0.004407	0.1201
BP2	65	71.53	112.8	0.7791	0.0004	0.07081
BP3	67.07	73.22	96.73	0	0.00738	0.06162
BP4	73.68	100.1	145.7	2.086	-0.004407	0.08925
BP6	72.14	109.5	154.8	0.01257	-0.00234	0.1171
BP7	76.55	134.6	174.4	1.948	0.0044	0.0314
BP8	70.91	148.7	175.9	0.4398	0.0058	0.122
BP9	56.78	166.2	178.2	0.5027	0.00338	0.08127
BP10	76.69	154.6	163	3.921	0.0096	0.02814
BP11	98.88	155	155.4	1.181	-0.0628	0.002737
BP12	58.31	171.1	173	0.5404	0.00762	0.00641
BP13	99.65	138.5	181.3	2.463	0.0532	0.001255
BP14	71.03	165.6	176	0.3393	0.00596	0.1184
BP15	71.03	217.7	218.7	0.7665	0.00214	0.1222
BP16	71.33	203.8	229.1	1.03	-0.00122	0.1221
BP18	147	194.6	197.4	0.387	-0.018	0.001772
BP19	165.8	190.1	196	2.768	-0.004	0.002841
BP20	191.8	198.4	199.7	1.508	0.008	0.008494
BP21	57.48	288	299.5	0.9299	0.00192	0.1195
BP22	71.42	247.2	258.4	1.043	-0.0032	0.122
BP23	62.69	162.4	190.8	2.639	0.0056	0.06404

Table 1. Low mass IDM benchmark points considered in the presented study, taken from [4]. In all benchmarks $m_h = 125.1\,\text{GeV}$. Bold font denotes BP for which H completely saturates DM relic density. Note that BP5 and BP17 were excluded by the updated XENON1T limits [56]. The values of the λ_{345} parameter for scenarios BP8 and BP22 were slightly modified with respect to [4], to be consistent with the most recent results on the relic density [54].

lower limit of 70 GeV for the charged scalar mass [41].[1] We also set a hard upper cutoff on the charged scalar life-time to avoid constraints from long-lived charged particle searches; a more detailed study of these constraints has recently been presented in [43]. We make use of recent LHC findings to constrain the total width of the Higgs particle [44], its invisible branching ratio [45] and the branching ratio $h \to \gamma\gamma$ [46].[2] In order to not overclose the universe the relic density of dark matter candidate H was required to be at most within a two sigma range of the value recently published by the Planck experiment, i.e. $\Omega_c h^2 \leq 0.1224$ [54]. Relic density has been calculated including all relevant channels, in particular decays into virtual gauge bosons. The proposed benchmarks have been selected

[1] In recent work [42], an additional recast has been presented which uses 13 TeV LHC data. We found that our benchmark points are not constrained by the limits derived in that reference.

[2] Additional tests of agreement with collider findings were performed using `HiggsBounds` [47–51] and `HiggsSignals` [52, 53].

JHEP07(2019)053

No.	m_H	m_A	$m_{H^\pm}$	λ_2	λ_{345}	$\Omega_c h^2$
HP1	176	291.4	312	1.49	-0.1035	0.0007216
HP2	557	562.3	565.4	4.045	-0.1385	0.07209
HP3	560	616.3	633.5	3.38	-0.0895	0.001129
HP4	571	676.5	682.5	1.98	-0.471	0.0005635
HP5	671	688.1	688.4	1.377	-0.1455	0.02447
HP6	713	716.4	723	2.88	0.2885	0.03515
HP7	807	813.4	818	3.667	0.299	0.03239
HP8	933	940	943.8	2.974	-0.2435	0.09639
HP9	935	986.2	988	2.484	-0.5795	0.002796
HP10	990	992.4	998.1	3.334	-0.040	0.122
HP11	250.5	265.5	287.2	3.908	-0.1501	0.00535
HP12	286.1	294.6	332.5	3.292	0.1121	0.00277
HP13	336	353.3	360.6	2.488	-0.1064	0.00937
HP14	326.6	331.9	381.8	0.02513	-0.06267	0.00356
HP15	357.6	400	402.6	2.061	-0.2375	0.00346
HP16	387.8	406.1	413.5	0.8168	-0.2083	0.0116
HP17	430.9	433.2	440.6	3.003	0.08299	0.0327
HP18	428.2	454	459.7	3.87	-0.2812	0.00858
HP19	467.9	488.6	492.3	4.122	-0.252	0.0139
HP20	505.2	516.6	543.8	2.538	-0.354	0.00887

Table 2. Additional set of high mass IDM benchmark points considered in the presented study, taken from [4]. In all benchmarks $m_h = 125.1\,\text{GeV}$. For HP10 scenario (bold) H completely saturates DM relic density; the value of the λ_{345} parameter for this scenario was slightly modified with respect to [4], to be consistent with the most recent results on the relic density [54].

(out of 13500 that passed all above criteria) to represent different signatures at e^+e^- colliders that differ e.g. in the mass spectrum or production cross sections, in order to cover a wide variety of possible collider signals. For the selected benchmark points, all of which correspond to masses of DM particles below 1 TeV, the Sommerfeld enhancement does not play a relevant role [55]. Finally the agreement with results from direct detection experiments [56] has been required.[3] As discussed in [4], constraints from indirect detection are weaker than direct detection constraints (see also e.g. discussion in [58]). The most stringent limits stem from indirect detection leading to $b\bar{b}$ final states [59]. These can be easily avoided by tuning the value of λ_{345}, which is irrelevant for the collider phenomenology discussed here. It should also be noted that dark matter predictions for some points, especially BP23, highly depend on the input in the SM mass spectrum; e.g. variations

[3]Electroweak higher-order corrections to direct detection cross section within the IDM have been presented in [57]. From that work, we can estimate the one-loop contributions for out benchmark points to be $\mathcal{O}\left(10^{-11}\text{ pb}\right)$. We explicitly checked that even assuming such a maximal additional contribution does not exclude any of our BPs.

JHEP07(2019)053

within 3 standard deviations for bottom and Higgs masses can lead to large variations in the predictions (up to a factor 5), while these are of no importance for our studies. In the scan presented in [4], we made use of the publicly available tools: the `2HDMC` code [60] and `micrOMEGAs` version 4.3.5 [61] to apply several of the constraints discussed above.

Prospects for detection at the LHC. In general, the IDM can be tested at the LHC through a variety of signatures, including mono-jet, mono-Z, mono-Higgs and Vector-Boson-Fusion + missing transverse energy signatures, as well as through multi-lepton and multi-jet final states, see discussions in [24, 25, 25, 28, 28, 62]. In [42], a dedicated discussion suggests that current searches, e.g. for multi-lepton final states, would have to be significantly modified in order to access the current IDM parameter space even for low dark matter masses. On the other hand, vector boson fusion production of an invisibly decaying Higgs [63] can already significantly constraint the models parameter space for $m_H \gtrsim 62.5\,\text{GeV}$. Depending on the channel, masses of DM particle up to 200–300 GeV would be accessible at the HL-LHC [25, 28, 62]. For the di-jet plus missing transverse energy signature, large background significantly affects LHC sensitivity.

Production cross sections for the benchmark points proposed here depend on the signature that is considered and can reach up to $\mathcal{O}$ (pb) at the 13 TeV LHC [64, 65]. An increase in center-of-mass energy to 27 TeV, as in the HE-LHC setup [66], can lead to an increase of an order of magnitude in production cross sections. However, without detailed experimental analyses, projections of reachability are difficult to make. We therefore strongly encourage the experimental collaborations to investigate the benchmark points presented here at current and future LHC runs.

3 Analyses strategies and simulation setup

In this work, we consider the following tree-level production processes of inert scalars at e^+e^- collisions[4]

$$\begin{aligned} e^+e^- &\to A\,H, \\ e^+e^- &\to H^+H^-. \end{aligned} \tag{3.1}$$

For the calculation of cross-sections as well as detailed signal and background simulation, we make use of the Monte Carlo event generator `WHizard 2.2.8` [67, 68]. For the signal, we employ the IDM model implemented in SARAH [69]. Model parameter files for the considered benchmark scenarios were prepared using `SPheno 4.0.3` [70, 71]. When generating signal and background events samples for the presented analysis, energy spectra for CLIC [72], based on detailed beam simulations, were taken into account. For initial state radiation (ISR), the intrinsic `WHizard` implementation of the lepton ISR structure function includes all orders of soft and soft-collinear photons as well as up to the third order in hard-collinear photons.

[4]The process $e^+e^- \to AA$ is in principle possible as well. However, this process is moderated by an s-channel SM Higgs and therefore highly suppressed by the electron Yukawa couplings.

JHEP07(2019)053

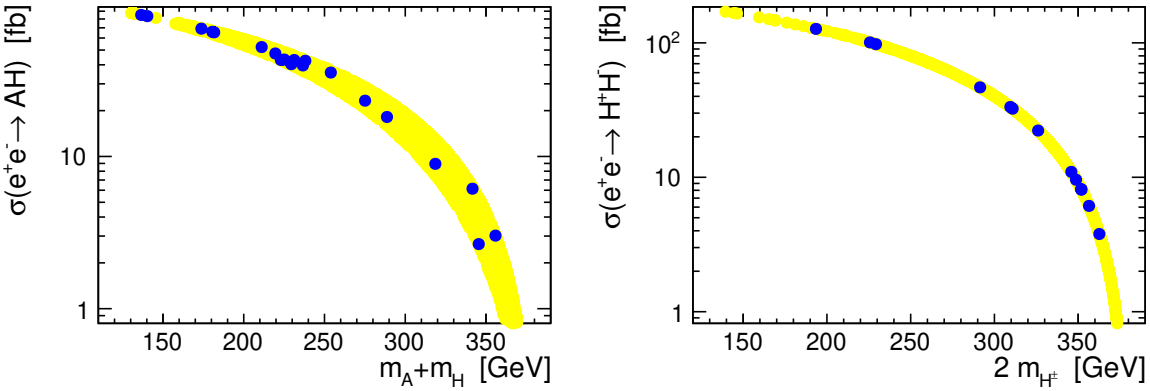

Figure 1. Leading-order cross-sections for neutral *(left)* and charged *(right)* inert scalar production, $e^+e^- \to HA$ and $e^+e^- \to H^+H^-$, for 380 GeV collision energy. The yellow band represents all scenarios selected in the model scan [4] while the blue dots represent the selected benchmark scenarios. Beam energy spectra are not included.

Leading-order cross-sections for the processes in (3.1) for 380 GeV collision energy, including initial state radiation, are presented in figure 1. In the scenarios considered in this paper the produced dark scalar A decays to a (real or virtual) Z boson and the (lighter) neutral scalar H, $A \to Z^{(\star)}H$, while the produced charged boson $H^\pm$ decays predominantly to a (real or virtual) $W^\pm$ boson and the neutral scalar H, $H^+ \to W^{\pm(\star)}H$, where the DM candidate H escapes detection. Since both the production and decay processes are governed by the SM electroweak couplings, the inert masses are the only BSM parameters probed at CLIC.

Since isolated leptons (electrons and muons) can be identified and reconstructed with very high efficiency and purity [72], we concentrate on Z and $W^\pm$ leptonic decays, leading to a signature of leptons and missing transverse energy. For the same flavour lepton pair signature, we restrict the analysis to the $\mu^+\mu^-$ final state, allowing for almost perfect reconstruction of lepton kinematics,[5] while for different flavour lepton pairs μ^+e^- and $e^+\mu^-$ final states are considered. We refrain from including detector effects in the results presented here as for the considered final states they are expected to only marginally change the outcome of our study. Muon pair production can be a signature of the AH production process followed by the A decay:

$$e^+e^- \to HA \;\to\; HHZ^{(\star)} \;\to\; HH\mu^+\mu^- \tag{3.2}$$

while the production of the different flavour lepton pair is the expected signature for H^+H^- production:

$$e^+e^- \to H^+H^- \;\to\; HHW^{+(*)}W^{-(*)} \;\to\; HH\ell^+\ell'^-\nu\bar{\nu}'. \tag{3.3}$$

Note that when both W bosons in (3.3) decay to muons, the charged Higgs pair production process will contribute to the signature (3.2) of HA production as well.

[5]For final state electrons energy resolution is affected by the final state radiation and bremsstrahlung effects [72].

JHEP07(2019)053

During simulations we do not constrain the intermediate particles, but consider all processes leading to $\ell^+ (\ell^-)' + \not{E}_\perp$. Especially processes with additional neutrinos can contribute and need to be taken into account. This includes processes with tau (pair) production and their successive leptonic decays.

To be specific, for processes with muons in the final state, the following processes have been simulated:

$$\begin{aligned} e^+e^- &\to \mu^+\mu^-\ HH, \\ &\to \mu^+\mu^-\nu_\mu\bar{\nu}_\mu\ HH, \\ &\to \tau^+\mu^-\nu_\tau\bar{\nu}_\mu\ HH,\ \ \mu^+\tau^-\nu_\mu\bar{\nu}_\tau\ HH, \\ &\to \tau^+\tau^-\ HH,\ \ \tau^+\tau^-\nu_\tau\bar{\nu}_\tau\ HH, \end{aligned}$$

where the final state taus are then forced to decay to a muon and a neutrino. For the background the following Standard Model processes are considered:

$$\begin{aligned} e^+e^- &\to \mu^+\mu^-, \\ &\to \mu^+\mu^-\ \nu_i\bar{\nu}_i, \\ &\to \tau^+\mu^-\ \nu_\tau\bar{\nu}_\mu,\ \mu^+\tau^-\ \nu_\mu\bar{\nu}_\tau, \\ &\to \tau^+\tau^-,\ \tau^+\tau^-\ \nu_i\bar{\nu}_i, \end{aligned}$$

where the additional neutrino pair can be of any flavour ($i = e, \mu, \tau$). As before, we generate all processes leading to the above final states, without constraining the intermediate particles states.

Similarly, for the electron-muon pair final state the following signal processes are considered:

$$\begin{aligned} e^+e^- &\to \mu^+\nu_\mu\, e^-\bar{\nu}_e\ HH,\ \ e^+\nu_e\, \mu^-\bar{\nu}_\mu\ HH, \\ &\to \mu^+\nu_\mu\, \tau^-\bar{\nu}_\tau\ HH,\ \ \tau^+\nu_\tau\, \mu^-\bar{\nu}_\mu\ HH, \\ &\to e^+\nu_e\, \tau^-\bar{\nu}_\tau\ HH,\ \ \tau^+\nu_\tau\, e^-\bar{\nu}_e\ HH, \\ &\to \tau^+\ \tau^-\ HH,\ \ \tau^+\nu_\tau\ \tau^-\bar{\nu}_\tau\ HH, \end{aligned}$$

with the final state tau leptons decaying to an electron or a muon (to match the required final state signature, μ^+e^- or $e^+\mu^-$). For the background in this case the following Standard Model four-fermion processes are considered:

$$\begin{aligned} e^+e^- &\to \mu^+\nu_\mu\, e^-\bar{\nu}_e\ ,\ e^+\nu_e\, \mu^-\bar{\nu}_\mu\ , \\ &\to \mu^+\nu_\mu\, \tau^-\bar{\nu}_\tau\ ,\ \tau^+\nu_\tau\, \mu^-\bar{\nu}_\mu, \\ &\to e^+\nu_e\, \tau^-\bar{\nu}_\tau\ ,\ \tau^+\nu_\tau\, e^-\bar{\nu}_e\ , \\ &\to \tau^+\tau^-,\ \tau^+\nu_\tau\, \tau^-\bar{\nu}_\tau\ . \end{aligned}$$

As mentioned above, beam energy spectra and ISR were taken into account.

Generator-level cuts corresponding to the expected detector acceptance were applied for both signal and background simulations: electrons or muons with energy of at least

JHEP07(2019)053

5 GeV need to be emitted at least 100 mrad from the beam direction and their angular separation should also be at least 100 mrad. To reduce background from radiative Z-return events we also require that there are no ISR photons emitted at angles above 100 mrad with energies larger that 10 GeV.

For the considered final states we assume that only two charged leptons are reconstructed in the detector. The observed final state can be completely described by a small set of kinematic variables. To assure the best possible discrimination between signal and background events, resulting in highest expected significance of the possible observation, we make use of multivariate analyses. We apply the Boosted Decision Tree (BDT) classification algorithm, as implemented in TMVA toolkit [73], with the following eight input variables describing the kinematics of the dilepton final state:

- total energy of the lepton pair, $\mathrm{E}_{\ell\ell}$;
- dilepton invariant mass, $M_{\ell\ell}$;
- dilepton transverse momentum, $\mathrm{p}_{\mathrm{T}}^{\ell\ell}$;
- polar angle of the dilepton pair, $\Theta_{\ell\ell}$;
- Lorentz boost of the dilepton pair, $\beta_{\ell\ell} = \mathrm{p}_{\ell\ell}/\mathrm{E}_{\ell\ell}$;
- reconstructed missing (recoil) mass M_{miss} (calculated assuming nominal e^+e^- collision energy);
- ℓ^- production angle with respect to the beam direction, calculated in the dilepton center-of-mass frame, $\Theta_{\ell}^{\star}$;
- ℓ^- production angle with respect to the dilepton pair boost direction, calculated in the dilepton center-of-mass frame, $\angle^{\star}(\ell, \ell\ell)$,

where lepton pair $\ell\ell$ denotes $\mu^+\mu^-$ for AH channel and μ^+e^- or $e^+\mu^-$ for H^+H^- production. The first five variables refer to the dilepton pair system as a whole, while the last two correspond to the single lepton polar angle calculated in the two different reference frames. Please note that these eight variables are not independent, as the final state with two massless leptons and missing energy only can be completely described by five parameters (plus azimuthal angle, which is not relevant). However, using more input variables resulted in better signal selection efficiencies. The BDT algorithm is trained individually for each benchmark scenario and each running energy using the generated event samples after detector acceptance and pre-selection cuts.

4 Inert scalars at the first stage of CLIC

First we investigate the discovery prospects for the IDM benchmarks at the initial CLIC operation at $\sqrt{s} = 380$ GeV with an expected integrated luminosity of 1 ab^{-1} [74].

The possibility to access benchmark points with $\sum m_i \geq 380$ GeV, that are not accessible at the first stage, is investigated in section 5, where the second and third energy

JHEP07(2019)053

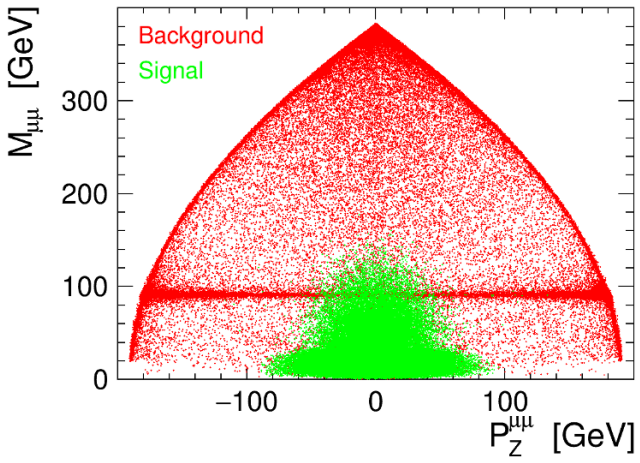

Figure 2. Distribution of the lepton pair invariant mass, $M_{\mu\mu}$, as a function of the lepton pair longitudinal momentum, $P_Z^{\mu\mu}$, for BP1 scenario (green points) and Standard Model background (red points). Same number of events were simulated for signal and background for centre-of-mass energy of 380 GeV, using CLIC luminosity spectra.

stages of CLIC, at 1.5 TeV and 3 TeV are considered with integrated luminosities of 2.5 and 5 ab^{-1}, respectively.

4.1 Neutral dark scalar pair production $e^+e^- \to AH$

As described above, in this channel we focus on final states with muon pairs and missing transverse energy. As the DM particles escape detection, the signal process will lead to large missing energy and momentum. Furthermore, the invariant mass of the lepton pair, stemming from the decay of a real or virtual Z boson, should be relatively small (depending on the mass splitting between A and H, but not greater than m_Z). On the other hand, the dominant Standard Model background process proceeds via the s-channel Z/γ di-muon production, with most pairs produced either with high invariant mass (events without hard ISR) or with significant longitudinal boost (events with high-energy ISR photon). We display the lepton pair invariant mass distribution for signal and background processes in figure 2. As expected, we observe that the event distribution for the signal (for the benchmark scenario BP1; green points) is concentrated on a much smaller range in the $P_z^{\mu\mu}, M^{\mu\mu}$ plane than the SM background distribution (red points). For the 380 GeV analysis we therefore require an invariant mass of the produced lepton pair to be below 100 GeV, and the absolute value of the longitudinal momentum below 140 GeV. These pre-selection cuts significantly reduce background from direct two fermion production, $e^+e^- \to \mu^+\mu^-$, hardly affecting the signal.

Shown in figure 3 are the distributions of the muon pair energy, $E_{\mu\mu}$, total transverse momentum, $p_T^{\mu\mu}$, polar angle, $\Theta_{\mu\mu}$, and the difference of the lepton azimuthal angles, $\cos\Delta\phi_{\mu\mu}$ for three benchmark scenarios with virtual Z boson production and the SM background. As the experimental signature is expected to depend on the mass difference

JHEP07(2019)053

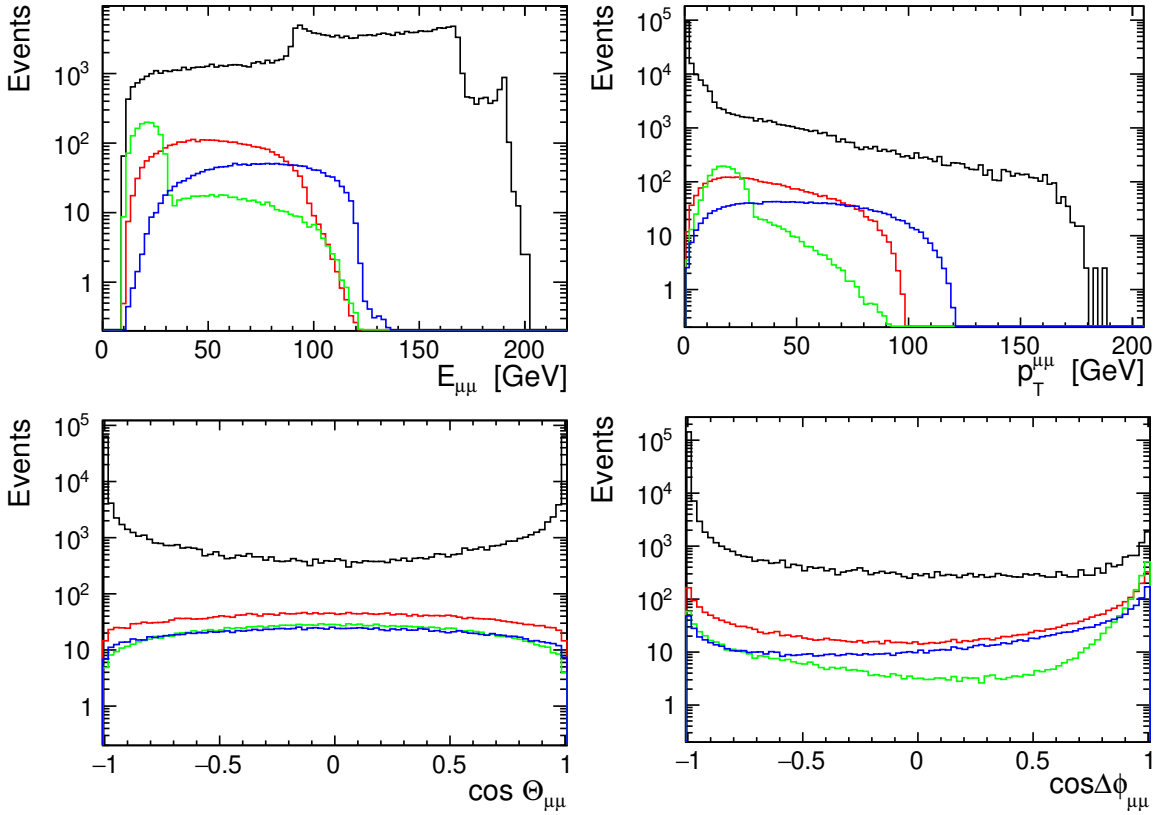

Figure 3. Distributions of the kinematic variables describing the leptonic final state considered in *AH* analysis: lepton pair energy, $E_{\mu\mu}$, total transverse momentum, $p_T^{\mu\mu}$, pair production angle, $\cos\Theta_{\mu\mu}$ and the difference of the lepton azimuthal angles, $\cos\Delta\phi_{\mu\mu}$. Expected distributions for representative benchmarks BP1 (red histogram), BP2 (green) and BP7 (blue) are compared with expected background (black histogram). Samples simulated for CLIC running at 380 GeV are normalised to 1 ab^{-1}.

between A and H states, we present benchmark points corresponding to different mass splittings: of about 6 GeV (BP2), 35 GeV (BP1) and 58 GeV (BP7). For low mass differences, the contribution from H^+H^- channel to the muon pair production signature is also clearly visible (a tail of events with higher lepton pair energy and transverse momentum).

Distributions of variables presented in figure 3 can be used to select signal-enhanced samples of events. The following selection requirements are therefore further imposed on the lepton pair:

- energy $E_{\mu\mu} < 100$ GeV,
- transverse momentum $p_T^{\mu\mu} > 10$ GeV,
- production angle (polar angle of the Z boson) $30° < \Theta_{\mu\mu} < 150°$,
- difference of the lepton azimuthal angles $|\Delta\varphi_{\mu\mu}| < \frac{\pi}{2}$.

Presented in figure 4 is the lepton pair invariant mass distribution after pre-selection and selection cuts. Signal samples for selected benchmark scenario and the background sample

JHEP07(2019)053

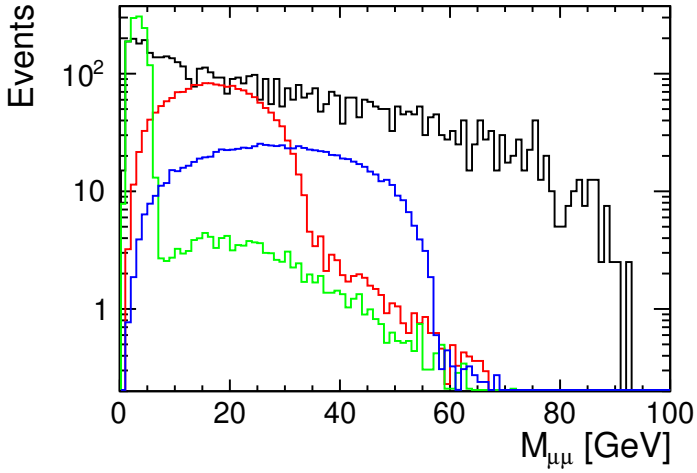

Figure 4. Distribution of the lepton pair invariant mass, $M_{\mu\mu}$, for BP1 (red histogram), BP2 (green) and BP7 (blue) signal scenarios, compared with expected Standard Model background (black histogram), after final event selection cuts (see text for details). Samples simulated for CLIC running at 380 GeV are normalised to $1\,\text{ab}^{-1}$.

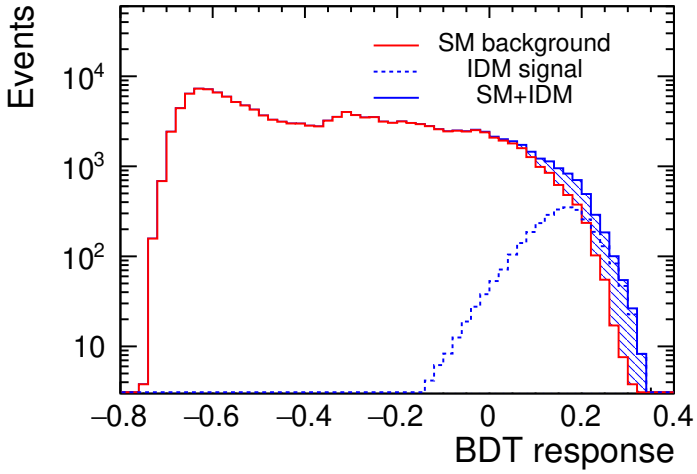

Figure 5. Response distributions of the BDT classifiers used for the selection of AH production events at CLIC, at $\sqrt{s} = 380\,\text{GeV}$. Signal samples for BP1 scenario and SM background are normalised to $1\,\text{ab}^{-1}$.

are normalised to $1\,\text{ab}^{-1}$. About 5400 background events are expected after all selection cuts, while 1810, 1290 and 540 signal events are expected for the BP1, BP2 and BP7 scenarios, respectively. This corresponds to about 21σ, 16σ and 7σ significance.

Higher signal significances are obtained making use of multivariate analyses after the application of pre-selection cuts. As an example, we show the BDT response distributions for BP1 (signal and SM background) in figure 5 for $1\,\text{ab}^{-1}$ collected at CLIC 380 GeV center-of-mass energy. The optimal significance is obtained for a BDT response cut of about 0.12, corresponding to 71% signal selection efficiency and 2.2% background selection efficiency, with a resulting signal significance of about 27.7σ. In figure 6 the significance

JHEP07(2019)053

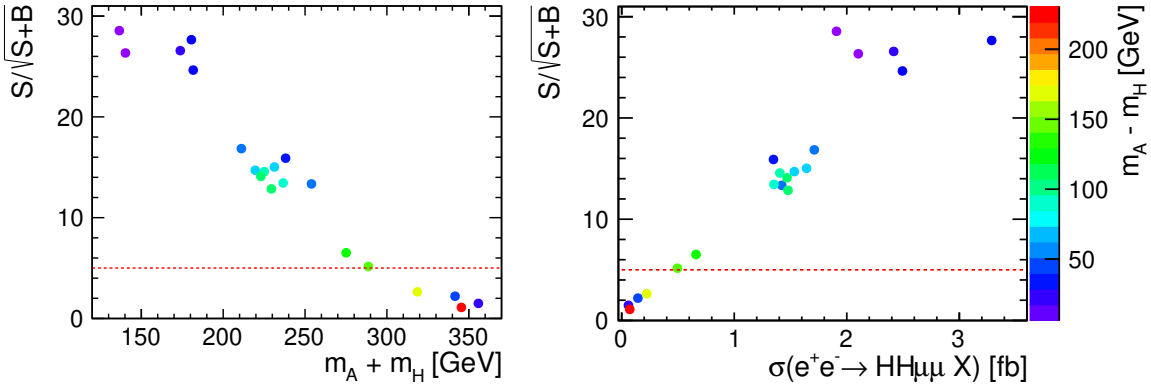

Figure 6. Expected significance of the deviations from the Standard Model predictions observed at 380 GeV CLIC for events with two muons in the final state ($\mu^+\mu^-$) as a function of the neutral inert scalar mass sum *(left)* and the production cross-section for the considered signal channel, after pre-selection cuts *(right)*, for the BPs from table 1. Color indicates the mass splitting between the A and H scalars (right scale applies to both plots).

using the above method is displayed as a function of the neutral inert scalar mass sum, $m_A + m_H$, and of the signal production cross-section for the considered final state, $\sigma(e^+e^- \to HH\mu^+\mu^- X_{\text{inv}})$. The expected significance is mainly related to the AH production cross-section. A discovery, corresponding to $5\,\sigma$, at the initial stage of CLIC is expected for scenarios with the signal cross-section (in the $\mu^+\mu^-$ channel, after pre-selection cuts on generator level) above about 0.5 fb, which corresponds to the neutral inert scalar mass sum below about 290 GeV. For the considered benchmark points we do not observe any sizable dependence of the expected significance on the mass splitting between the two neutral scalars, $m_A - m_H$ (indicated by colour scale in figure 6).

4.2 Charged scalar pair production $e^+e^- \to H^+H^-$

The selection of H^+H^- production events is more challenging than for the AH channel, as the two leptons in the final state no longer originate from a single (on- or off-shell) intermediate state. We therefore do not apply any additional pre-selection cuts (except for the detector acceptance cuts, as described in section 3). However, this also allows us to consider the electron-muon pairs in the final state, avoiding large SM background from the direct lepton pair production ($e^+e^- \to \ell^+\ell^-$; this channel contributes only via leptonic tau decays, suppressed by the corresponding branching fractions).

With only the detector acceptance cuts on the generator level, the expected background cross-section for the considered final state is about 500 fb, over two orders of magnitude higher than for the considered benchmark points. However, kinematic distributions are very different, as two massive scalars are produced in the signal case, reducing the kinematic space available for lepton pair production. In figure 7 distributions of the selected variables describing the leptonic final state for three benchmark scenarios (BP1, BP3 and BP6) are compared with Standard Model expectations. Clear differences between the signal and background distributions allow for efficient selection of signal-enhanced sample of events using the multivariate analysis. We follow the same procedure and the same set of

JHEP07(2019)053

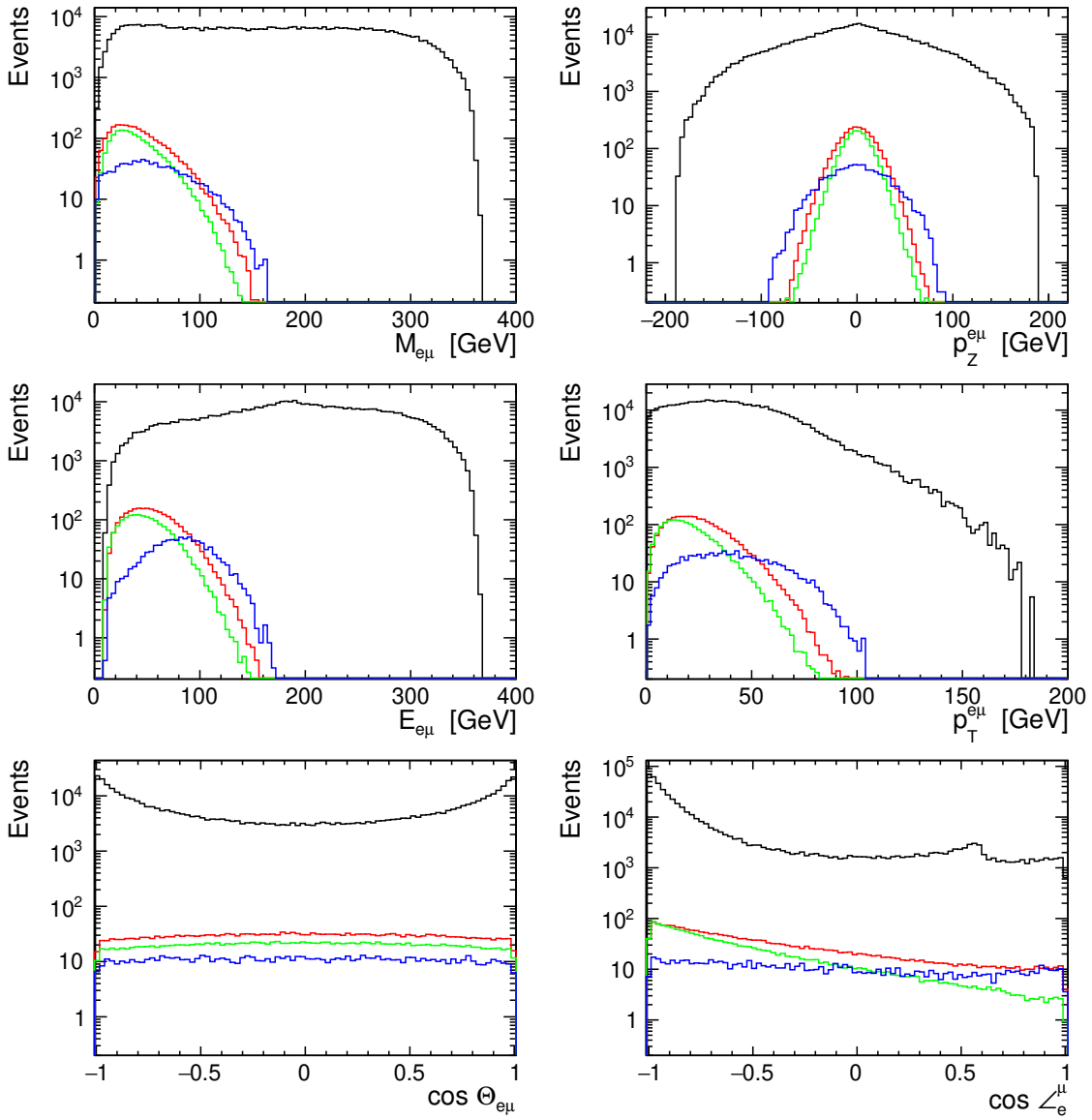

Figure 7. Distributions of the kinematic variables describing the leptonic final state considered in H^+H^- analysis: lepton pair invariant mass, $M_{e\mu}$, total longitudinal momentum, $P_Z^{e\mu}$, lepton pair energy, $E_{e\mu}$, total transverse momentum, $P_T^{e\mu}$, pair production angle, $\Theta_{e\mu}$ and the angular distance between the two leptons, $\cos\angle_e^\mu$. Expected distributions for BP1 (red histogram), BP3 (green) and BP6 (blue) are compared with expected background (black histogram). Samples simulated for CLIC running at 380 GeV are normalised to 1 ab^{-1}.

input variables is used as for the AH analysis described above. The BDT classification algorithm is trained separately for each benchmark point to discriminate between signal and background processes. Examples of the BDT response distributions for the BP1 signal sample and SM background samples simulated for 1 ab^{-1} at 380 GeV CLIC are shown in figure 8. While due to a large SM background it is not possible to select the signal-dominated sample based on the BDT response, the highest significance is obtained when

JHEP07(2019)053

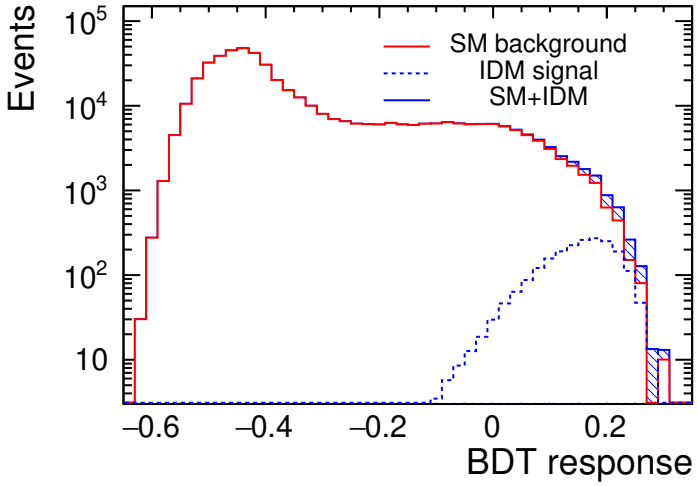

Figure 8. Response distributions of the BDT classifiers used for the selection of H^+H^- production events at CLIC, at $\sqrt{s} = 380\,\text{GeV}$. Signal sample for BP1 scenario and SM background are normalised to $1\,\text{ab}^{-1}$.

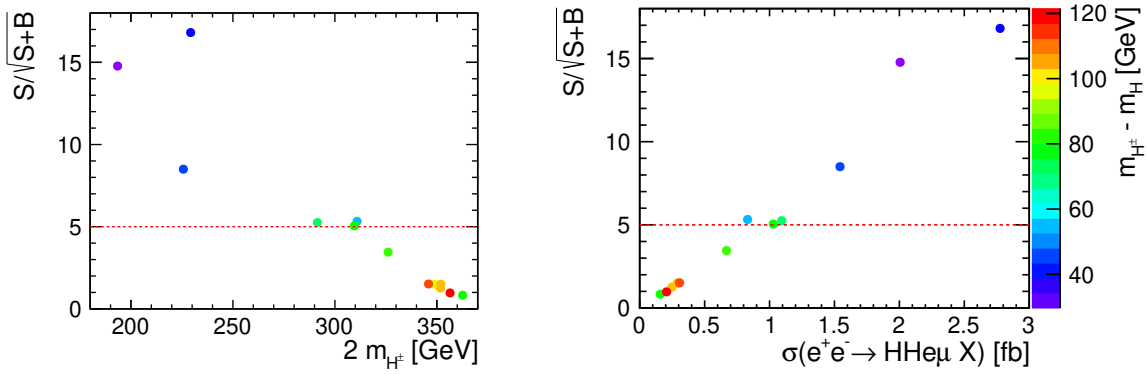

Figure 9. Expected significance of the deviations from the Standard Model predictions observed at 380 GeV CLIC for events with electron-muon pair in the final state ($e^+\mu^-$ or μ^+e^-) as a function of twice the charged scalar mass *(left)* and the production cross-section for the considered signal channel *(right)*, for different IDM benchmark points. Color indicates the mass splitting between the $H^\pm$ and H scalars (right scale applies to both plots).

selecting events with BDT response above 0.12. About 1700 signal events are expected in the final sample (BDT selection efficiency of 70%) with background contribution of about 8500 events (BDT selection efficiency of 1.7%), resulting in the significance of the observation of about 17σ.

As was the case for the AH channel, the expected significance of the $e\mu$ signal is mainly related to the production cross-section for the considered channel. This is shown in figure 9, where the expected significance for the electron-muon final state ($e^+\mu^-$ or μ^+e^-) are plotted as a function of $2m_{H^\pm}$ (left panel) and the production cross-section (right panel), for different IDM benchmark points. Discovery at the initial stage of CLIC is only possible for scenarios with signal cross-sections (in the electron-muon channel) above about 1 fb. This

JHEP07(2019)053

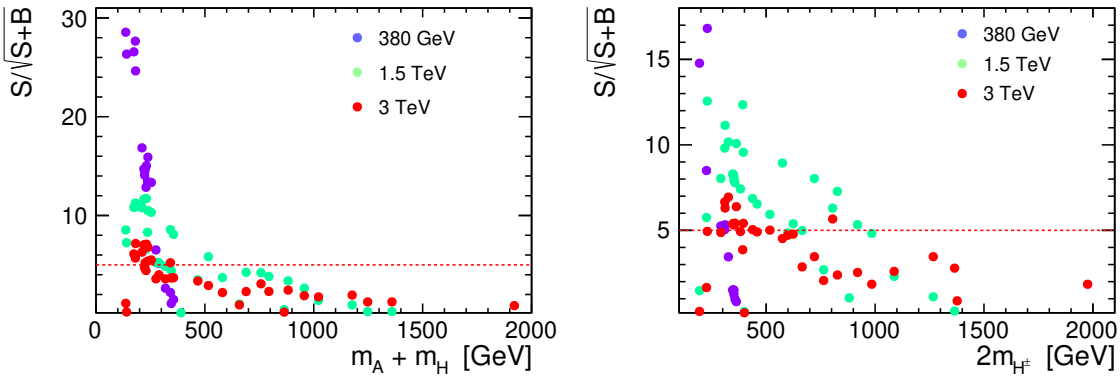

Figure 10. Significance of the deviations from the Standard Model predictions expected at the subsequent CLIC stages for: *(left)* events with two muons in the final state ($\mu^+\mu^-$) as a function of the sum of neutral inert scalar masses and *(right)* events with an electron and a muon in the final state ($e^+\mu^-$ or $e^-\mu^+$) as a function of twice the charged scalar mass, for IDM benchmark points in tables 1 and 2.

corresponds to charged scalar masses below roughly 150 GeV. We do not observe any sizable dependence of the expected significance on the mass splitting between the charged and neutral inert scalars, $m_{H^\pm} - m_H$ (indicated by colour scale in figure 9), within the considered range of parameters. Reduced signal channel cross section and thus reduced signal sensitivity observed for one of the benchmark points in figure 9 (BP2 with $m_{H^\pm} = 112.8\,\text{GeV}$) is due to the significant contribution of cascade decays, $H^\pm \to W^{\pm\star}A \to W^{\pm\star}Z^\star H$, which were not considered in the signal event selection.

5 Inert scalars at high-energy stages of CLIC

We now turn to the discovery prospects of the two high-energy stages at 1.5 TeV and 3 TeV with assumed integrated luminosities of $2.5\,\text{ab}^{-1}$ and $5\,\text{ab}^{-1}$ [74]. The same analysis procedure described in section 4 was applied to signal and background samples simulated for high-energy CLIC stages. As before, proper energy spectra for CLIC [72], based on detailed beam simulations, were taken into account, which is crucial for a correct description of signal and background at high collider energies. We applied the same generator-level cuts as before, but did not make use of any additional pre-selection cuts. Furthermore, we extend our study to include additional high-mass benchmark points not accessible at 380 GeV; these are listed in table 2.

In figure 10, we display the expected significances of the IDM signal in the AH and H^+H^- channel as a function of the inert scalar masses for subsequent CLIC running stages. For the AH channel (muon-pair production), increasing the running energy and integrated luminosity results in only a moderate extension of the discovery potential of CLIC. With $2.5\,\text{ab}^{-1}$ at 1.5 TeV scenarios with the sum of neutral inert scalar masses up to about 550 GeV can be probed, compared to about 290 GeV for 380 GeV running. Prospects for high-energy CLIC running look significantly better if the H^+H^- production with the electron-muon final state is considered. Here the expected signal significance

JHEP07(2019)053

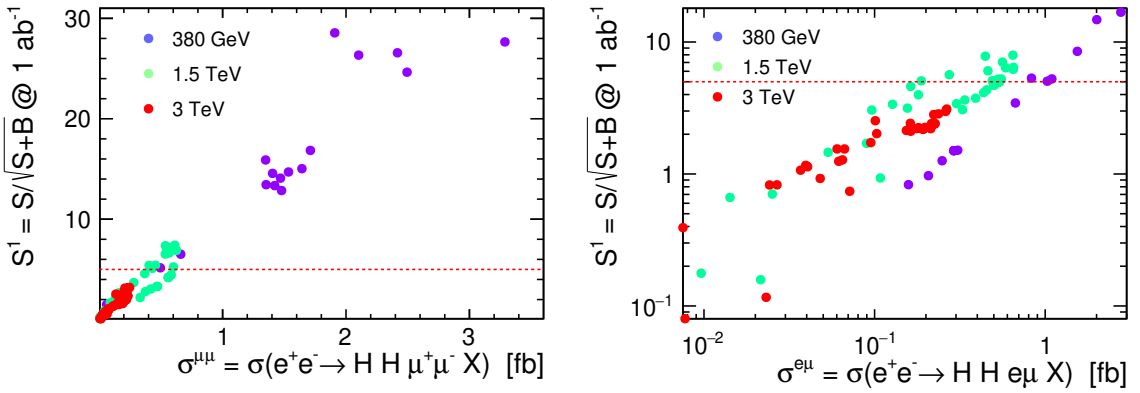

Figure 11. Significance of the deviations from the Standard Model predictions expected at different CLIC running stages, assuming the same integrated luminosity of $1\,\text{ab}^{-1}$, as a function of the signal cross-section in the considered channel, for: *(left)* events with two muons in the final state ($\mu^+\mu^-$) and *(right)* events with electron-muon pair production ($e^+\mu^-$ or $e^-\mu^+$), for the IDM benchmark points in tables 1 and 2.

decreases much slower with the charged scalar mass and we can probe masses up to about 500 GeV at 1.5 TeV, compared to 150 GeV at the first CLIC stage (see figure 10 right panel).

The significance is mainly driven by the signal production cross section and is approximately proportional to the square-root of the integrated luminosity. For parameter points that are already accessible at Stage 1 the AH production cross sections decrease with the collision energy much faster than most of the backgrounds and the significance of observation decreases at Stage 2. Only for points with $m_A + m_H \gtrsim 300\,\text{GeV}$, which are close to the production threshold at Stage 1, higher integrated luminosity and the production cross sections enhanced by up to a factor of 2 result in better sensitivity at center-of-mass energy of 1.5 TeV. Similarly, when going from 1.5 TeV to 3 TeV, the significance of observation increases only for scenarios with $m_A + m_H \gtrsim 1.2\,\text{TeV}$.

As we search for the signal contribution on top of a much larger background, we expect that the significance is (to a first approximation) proportional to the square-root of the integrated luminosity. In order to compare the CLIC sensitivity to the IDM benchmark scenarios at different energies, we scale the expected significance at high-energy stages to the integrated luminosity of $1\,\text{ab}^{-1}$ assumed for 380 GeV running. This allows us to separate luminosity and cross-section contributions to the overall significance, and will also allow for projections of the discovery potential at arbitrary luminosities.

In figure 11, we show the scaled significance results, presented as a function of the signal production cross-section. For the AH channel, which leads to $\mu^+\mu^-$ final states, a universal linear dependence on the signal cross-section is observed which does not seem to depend on the running energy. Significant (above 5σ) observation is possible for cross-sections roughly larger than 0.5 fb (for higher luminosities, these should be rescaled by $\sqrt{1\,/\mathcal{L}\cdot\,\text{ab}}$).

For the H^+H^- channel, however, leading to $e^\pm\mu^\mp$ final states, the high-energy running of CLIC clearly gives better sensitivity to heavy IDM scenarios (for points with similar production cross-section and assuming same luminosity) than the initial CLIC stage

JHEP07(2019)053

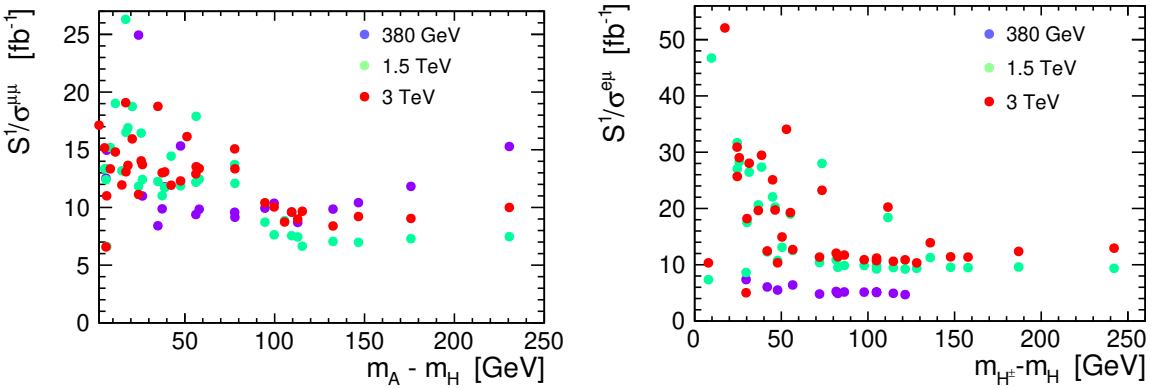

Figure 12. Ratio of the expected significance scaled to the integrated luminosity of $1\,\text{ab}^{-1}$ to the signal cross-section in the considered channel: *(left)* with two muons in the final state ($\mu^+\mu^-$) and *(right)* with electron-muon pair production ($e^+\mu^-$ or $e^-\mu^+$), as a function of the scalar mass differences, for different IDM benchmark points.

(see figure 11 right). The relatively large differences between different BPs with similar cross-sections at the same center-of-mass energies originate from the mass scale of the heavy scalars.

Finally, we investigate the dependence of the signal significance on the mass difference between neutral/charged inert scalar and the DM candidate. In figure 12, we show the ratio of the expected significance (scaled to the integrated luminosity of $1\,\text{ab}^{-1}$) to the signal cross-section in the considered channel, as a function of the corresponding scalar mass difference. This ratio indicates the expected significance for the particular mass splitting, assuming the reference signal channel cross section of 1 fb. For AH production (muon-pair channel) at high-energy stages, the experimental sensitivity seems to be significantly better for low mass differences, below m_Z, when the virtual Z boson is produced in the A boson decay, $A \to Z^{(\star)}H$. This is because signal events can be better separated from the SM backgrounds for such scenarios. One can also note that for high mass differences, $m_A - m_H > m_Z$, the experimental sensitivity is clearly better for low-energy running.

The situation is similar for the H^+H^- production signal in the electron-muon channel. For high running energies, a better sensitivity is expected for low mass differences when the virtual $W^\pm$ boson is produced in the charged scalar decay. However, it is also clear that the experimental sensitivity is much better at high-energy running than at the first CLIC stage and this observation does not depend on the considered dark scalar mass difference.

The results presented in figure 10 seem to indicate that many high mass IDM scenarios will remain inaccessible at CLIC, even at high energies. However, one has to stress that this is mainly due to the small branching ratios for the considered leptonic final states: 3.3% for $AH \to HH\mu^+\mu^-$ and 2.3% for $H^+H^- \to HH\mu^\pm e^\mp\nu\nu$. For scenarios where the signal cross sections in the dilepton channel are too small, it might be worthwhile to investigate semi-leptonic decays in the H^+H^- production channel. Due to the much larger branching ratios (28.6% for $H^+H^- \to HH\ell^\pm\nu qq'$, with $\ell = e, \mu$) the expected number of H^+H^- signal events in the semi-leptonic final state is over an order of magnitude larger than for

JHEP07(2019)053

the electron-muon signature. As a similar scaling is expected for the background processes (dominated by the W^+W^- production), we expect that the significance of the observation in the semi-leptonic channel should be increased by at least a factor of 3 (corresponding to the ten-fold increase of the integrated luminosity). An investigation in this channel could furthermore profit from a full reconstruction of the $W^\pm$ that decays hadronically, which allows to use the reconstructed W boson mass and energy as additional discriminators in the BDT algorithm. However, a proper estimate of the expected significance for this case would require a much more detailed analysis, including parton showering, hadronisation and detector response simulation, and event reconstruction with particle flow algorithm and final state reconstruction using accurate jet clustering and lepton identification processes. This is beyond the scope of the work presented here.

6 Conclusions

In this work, we have studied prospects for discovery of inert scalars of the Inert Doublet Model at CLIC running at 380 GeV, 1.5 TeV and 3 TeV. A set of benchmark points, proposed in [4] and satisfying all experimental and theoretical constraints, has been considered. We focused on pair-production of charged dark scalars $H^+ H^-$ and production of the DM candidate with the second neutral scalar boson, HA, with subsequent decays to leptonic final states. Signal and background event samples were generated with `WHizard 2.2.8`, taking into account all processes that lead to the considered final states. Signatures for production of new scalars were searched for in the kinematic distributions for events with exclusive production of two muons or an electron and a muon. Significance of the possible observation was studied using multivariate analysis methods.

We found that most of the low-mass benchmark scenarios proposed in [4] can be observed with high significance in the di-muon channel already with $1\,\text{ab}^{-1}$ collected at 380 GeV (the first stage of CLIC), provided that the sum of neutral inert scalar masses, $m_A + m_H < 290\,\text{GeV}$. Similar constraints also apply to the observation of the charged scalar pair-production (electron-muon pair-production channel), which is however fulfilled for fewer scenarios.

Scenarios which are not kinematically accessible at the first stage of CLIC can be searched for at high-energy stages, at 1.5 TeV and 3 TeV. The signal production cross-section for both considered channels decreases significantly with energy, much faster than for the corresponding background processes. Signal cross sections for the considered final states are further reduced by the small branching fractions for the dilepton channels. We found that at 1.5 TeV the discovery reach is extended to the sum of scalar masses of about 550 GeV in the dimuon channel and for charged scalar masses up to about 500 GeV in the $e^\pm \mu^\mp$ channels. For the scenarios considered here, increasing the center-of-mass energy to 3 TeV does not significantly improve the sensitivity. Therefore, the observation of the inert scalar production in the leptonic channels will be challenging at high-energy CLIC and a significant signal is only expected for relatively low masses. However, higher significance and the discovery reach extending up to the kinematic limit could be expected for H^+H^- production in the semi-leptonic final state (isolated lepton and a pair of jets or one massive jet). This is in the line of future work.

JHEP07(2019)053

Acknowledgments

This research was supported in parts by the National Science Centre, Poland, the HARMONIA project under contract UMO-2015/18/M/ST2/00518 (2016–2019) and OPUS project under contract UMO-2017/25/B/ST2/00496 (2018–2021), as well as the COST Action CA15108. TR was supported by Michigan State University through computational resources provided by the Institute for Cyber-Enabled Research, by grant K 125105 of the National Research, Development and Innovation Fund in Hungary, and by the European Union through the European Regional Development Fund — the Competitiveness and Cohesion Operational Programme (KK.01.1.1.06). TR also thanks the Galileo Galilei Institute for Theoretical Physics for the hospitality and the INFN for partial support during the completion of this work. The work of WK was partially supported by the German Research Foundation (DFG) under grants number STO 876/4-1 and STO 876/2-2. JK and WK thank Gudrid Moortgat-Pick for her hospitality and the DFG for a partial support through the SFB 676 "Particles, Strings and the Early Universe" during the initial stage of this project.

References

[1] N.G. Deshpande and E. Ma, *Pattern of Symmetry Breaking with Two Higgs Doublets*, *Phys. Rev.* **D 18** (1978) 2574 [INSPIRE].

[2] Q.-H. Cao, E. Ma and G. Rajasekaran, *Observing the Dark Scalar Doublet and its Impact on the Standard-Model Higgs Boson at Colliders*, *Phys. Rev.* **D 76** (2007) 095011 [arXiv:0708.2939] [INSPIRE].

[3] R. Barbieri, L.J. Hall and V.S. Rychkov, *Improved naturalness with a heavy Higgs: An Alternative road to LHC physics*, *Phys. Rev.* **D 74** (2006) 015007 [hep-ph/0603188] [INSPIRE].

[4] J. Kalinowski, W. Kotlarski, T. Robens, D. Sokolowska and A.F. Żarnecki, *Benchmarking the Inert Doublet Model for e^+e^- colliders*, *JHEP* **12** (2018) 081 [arXiv:1809.07712] [INSPIRE].

[5] L. Lopez Honorez, E. Nezri, J.F. Oliver and M.H.G. Tytgat, *The Inert Doublet Model: An Archetype for Dark Matter*, *JCAP* **02** (2007) 028 [hep-ph/0612275] [INSPIRE].

[6] E. Lundstrom, M. Gustafsson and J. Edsjo, *The Inert Doublet Model and LEP II Limits*, *Phys. Rev.* **D 79** (2009) 035013 [arXiv:0810.3924] [INSPIRE].

[7] E. Dolle, X. Miao, S. Su and B. Thomas, *Dilepton Signals in the Inert Doublet Model*, *Phys. Rev.* **D 81** (2010) 035003 [arXiv:0909.3094] [INSPIRE].

[8] E.M. Dolle and S. Su, *The Inert Dark Matter*, *Phys. Rev.* **D 80** (2009) 055012 [arXiv:0906.1609] [INSPIRE].

[9] L. Lopez Honorez and C.E. Yaguna, *The inert doublet model of dark matter revisited*, *JHEP* **09** (2010) 046 [arXiv:1003.3125] [INSPIRE].

JHEP07(2019)053

[10] X. Miao, S. Su and B. Thomas, *Trilepton Signals in the Inert Doublet Model*, *Phys. Rev.* **D 82** (2010) 035009 [arXiv:1005.0090] [INSPIRE].

[11] M. Gustafsson, S. Rydbeck, L. Lopez-Honorez and E. Lundstrom, *Status of the Inert Doublet Model and the Role of multileptons at the LHC*, *Phys. Rev.* **D 86** (2012) 075019 [arXiv:1206.6316] [INSPIRE].

[12] A. Arhrib, R. Benbrik and N. Gaur, $H \to \gamma\gamma$ *in Inert Higgs Doublet Model*, *Phys. Rev.* **D 85** (2012) 095021 [arXiv:1201.2644] [INSPIRE].

[13] B. Swiezewska and M. Krawczyk, *Diphoton rate in the inert doublet model with a 125 GeV Higgs boson*, *Phys. Rev.* **D 88** (2013) 035019 [arXiv:1212.4100] [INSPIRE].

[14] M. Aoki, S. Kanemura and H. Yokoya, *Reconstruction of Inert Doublet Scalars at the International Linear Collider*, *Phys. Lett.* **B 725** (2013) 302 [arXiv:1303.6191] [INSPIRE].

[15] S.-Y. Ho and J. Tandean, *Probing Scotogenic Effects in e^+e^- Colliders*, *Phys. Rev.* **D 89** (2014) 114025 [arXiv:1312.0931] [INSPIRE].

[16] A. Arhrib, Y.-L.S. Tsai, Q. Yuan and T.-C. Yuan, *An Updated Analysis of Inert Higgs Doublet Model in light of the Recent Results from LUX, PLANCK, AMS-02 and LHC*, *JCAP* **06** (2014) 030 [arXiv:1310.0358] [INSPIRE].

[17] M. Krawczyk, D. Sokolowska, P. Swaczyna and B. Swiezewska, *Constraining Inert Dark Matter by $R_{\gamma\gamma}$ and WMAP data*, *JHEP* **09** (2013) 055 [arXiv:1305.6266] [INSPIRE].

[18] A. Goudelis, B. Herrmann and O. Stål, *Dark matter in the Inert Doublet Model after the discovery of a Higgs-like boson at the LHC*, *JHEP* **09** (2013) 106 [arXiv:1303.3010] [INSPIRE].

[19] I.F. Ginzburg, *Measuring mass and spin of Dark Matter particles with the aid energy spectra of single lepton and dijet at the e^+e^- Linear Collider*, *J. Mod. Phys.* **5** (2014) 1036 [arXiv:1410.0869] [INSPIRE].

[20] G. Bélanger, B. Dumont, A. Goudelis, B. Herrmann, S. Kraml and D. Sengupta, *Dilepton constraints in the Inert Doublet Model from Run 1 of the LHC*, *Phys. Rev.* **D 91** (2015) 115011 [arXiv:1503.07367] [INSPIRE].

[21] N. Blinov, J. Kozaczuk, D.E. Morrissey and A. de la Puente, *Compressing the Inert Doublet Model*, *Phys. Rev.* **D 93** (2016) 035020 [arXiv:1510.08069] [INSPIRE].

[22] A. Arhrib, R. Benbrik, J. El Falaki and A. Jueid, *Radiative corrections to the Triple Higgs Coupling in the Inert Higgs Doublet Model*, *JHEP* **12** (2015) 007 [arXiv:1507.03630] [INSPIRE].

[23] A. Ilnicka, M. Krawczyk and T. Robens, *Inert Doublet Model in light of LHC Run I and astrophysical data*, *Phys. Rev.* **D 93** (2016) 055026 [arXiv:1508.01671] [INSPIRE].

[24] P. Poulose, S. Sahoo and K. Sridhar, *Exploring the Inert Doublet Model through the dijet plus missing transverse energy channel at the LHC*, *Phys. Lett.* **B 765** (2017) 300 [arXiv:1604.03045] [INSPIRE].

[25] A. Datta, N. Ganguly, N. Khan and S. Rakshit, *Exploring collider signatures of the inert Higgs doublet model*, *Phys. Rev.* **D 95** (2017) 015017 [arXiv:1610.00648] [INSPIRE].

[26] S. Kanemura, M. Kikuchi and K. Sakurai, *Testing the dark matter scenario in the inert doublet model by future precision measurements of the Higgs boson couplings*, *Phys. Rev.* **D 94** (2016) 115011 [arXiv:1605.08520] [INSPIRE].

JHEP07(2019)053

[27] A.G. Akeroyd et al., *Prospects for charged Higgs searches at the LHC*, *Eur. Phys. J.* **C 77** (2017) 276 [arXiv:1607.01320] [INSPIRE].

[28] N. Wan et al., *Searches for Dark Matter via Mono-W Production in Inert Doublet Model at the LHC*, *Commun. Theor. Phys.* **69** (2018) 617 [INSPIRE].

[29] A. Ilnicka, T. Robens and T. Stefaniak, *Constraining Extended Scalar Sectors at the LHC and beyond*, *Mod. Phys. Lett.* **A 33** (2018) 1830007 [arXiv:1803.03594] [INSPIRE].

[30] A. Belyaev et al., *Advancing LHC probes of dark matter from the inert two-Higgs-doublet model with the monojet signal*, *Phys. Rev.* **D 99** (2019) 015011 [arXiv:1809.00933] [INSPIRE].

[31] S. Nie and M. Sher, *Vacuum stability bounds in the two Higgs doublet model*, *Phys. Lett.* **B 449** (1999) 89 [hep-ph/9811234] [INSPIRE].

[32] I.F. Ginzburg, K.A. Kanishev, M. Krawczyk and D. Sokolowska, *Evolution of Universe to the present inert phase*, *Phys. Rev.* **D 82** (2010) 123533 [arXiv:1009.4593] [INSPIRE].

[33] M.S. Chanowitz and M.K. Gaillard, *The TeV Physics of Strongly Interacting W's and Z's*, *Nucl. Phys.* **B 261** (1985) 379 [INSPIRE].

[34] I.F. Ginzburg and I.P. Ivanov, *Tree-level unitarity constraints in the most general 2HDM*, *Phys. Rev.* **D 72** (2005) 115010 [hep-ph/0508020] [INSPIRE].

[35] GFITTER GROUP collaboration, *The global electroweak fit at NNLO and prospects for the LHC and ILC*, *Eur. Phys. J.* **C 74** (2014) 3046 [arXiv:1407.3792] [INSPIRE].

[36] G. Altarelli and R. Barbieri, *Vacuum polarization effects of new physics on electroweak processes*, *Phys. Lett.* **B 253** (1991) 161 [INSPIRE].

[37] M.E. Peskin and T. Takeuchi, *A New constraint on a strongly interacting Higgs sector*, *Phys. Rev. Lett.* **65** (1990) 964 [INSPIRE].

[38] M.E. Peskin and T. Takeuchi, *Estimation of oblique electroweak corrections*, *Phys. Rev.* **D 46** (1992) 381 [INSPIRE].

[39] I. Maksymyk, C.P. Burgess and D. London, *Beyond S, T and U*, *Phys. Rev.* **D 50** (1994) 529 [hep-ph/9306267] [INSPIRE].

[40] PARTICLE DATA GROUP collaboration, *Review of Particle Physics*, *Phys. Rev.* **D 98** (2018) 030001 [INSPIRE].

[41] A. Pierce and J. Thaler, *Natural Dark Matter from an Unnatural Higgs Boson and New Colored Particles at the TeV Scale*, *JHEP* **08** (2007) 026 [hep-ph/0703056] [INSPIRE].

[42] D. Dercks and T. Robens, *Constraining the Inert Doublet Model using Vector Boson Fusion*, arXiv:1812.07913 [INSPIRE].

[43] J. Heisig, S. Kraml and A. Lessa, *Constraining new physics with searches for long-lived particles: Implementation into SModelS*, *Phys. Lett.* **B 788** (2019) 87 [arXiv:1808.05229] [INSPIRE].

[44] CMS collaboration, *Measurements of the Higgs boson width and anomalous HVV couplings from on-shell and off-shell production in the four-lepton final state*, *Phys. Rev.* **D 99** (2019) 112003 [arXiv:1901.00174] [INSPIRE].

[45] CMS collaboration, *Searches for invisible decays of the Higgs boson in pp collisions at* $\sqrt{s} = 7$, 8 *and* 13 *TeV*, *JHEP* **02** (2017) 135 [arXiv:1610.09218] [INSPIRE].

JHEP07(2019)053

[46] ATLAS and CMS collaborations, *Measurements of the Higgs boson production and decay rates and constraints on its couplings from a combined ATLAS and CMS analysis of the LHC pp collision data at $\sqrt{s} = 7$ and 8 TeV*, *JHEP* **08** (2016) 045 [arXiv:1606.02266] [INSPIRE].

[47] P. Bechtle, O. Brein, S. Heinemeyer, G. Weiglein and K.E. Williams, *HiggsBounds: Confronting Arbitrary Higgs Sectors with Exclusion Bounds from LEP and the Tevatron*, *Comput. Phys. Commun.* **181** (2010) 138 [arXiv:0811.4169] [INSPIRE].

[48] P. Bechtle, O. Brein, S. Heinemeyer, G. Weiglein and K.E. Williams, *HiggsBounds 2.0.0: Confronting Neutral and Charged Higgs Sector Predictions with Exclusion Bounds from LEP and the Tevatron*, *Comput. Phys. Commun.* **182** (2011) 2605 [arXiv:1102.1898] [INSPIRE].

[49] P. Bechtle et al., *Recent Developments in HiggsBounds and a Preview of HiggsSignals*, PoS(CHARGED2012)024 (2012) [arXiv:1301.2345] [INSPIRE].

[50] P. Bechtle et al., *HiggsBounds-4: Improved Tests of Extended Higgs Sectors against Exclusion Bounds from LEP, the Tevatron and the LHC*, *Eur. Phys. J.* **C 74** (2014) 2693 [arXiv:1311.0055] [INSPIRE].

[51] P. Bechtle, S. Heinemeyer, O. Stal, T. Stefaniak and G. Weiglein, *Applying Exclusion Likelihoods from LHC Searches to Extended Higgs Sectors*, *Eur. Phys. J.* **C 75** (2015) 421 [arXiv:1507.06706] [INSPIRE].

[52] P. Bechtle, S. Heinemeyer, O. Stål, T. Stefaniak and G. Weiglein, *HiggsSignals: Confronting arbitrary Higgs sectors with measurements at the Tevatron and the LHC*, *Eur. Phys. J.* **C 74** (2014) 2711 [arXiv:1305.1933] [INSPIRE].

[53] P. Bechtle, S. Heinemeyer, O. Stål, T. Stefaniak and G. Weiglein, *Probing the Standard Model with Higgs signal rates from the Tevatron, the LHC and a future ILC*, *JHEP* **11** (2014) 039 [arXiv:1403.1582] [INSPIRE].

[54] PLANCK collaboration, *Planck 2018 results. VI. Cosmological parameters*, arXiv:1807.06209 [INSPIRE].

[55] C. Garcia-Cely, M. Gustafsson and A. Ibarra, *Probing the Inert Doublet Dark Matter Model with Cherenkov Telescopes*, *JCAP* **02** (2016) 043 [arXiv:1512.02801] [INSPIRE].

[56] XENON collaboration, *Dark Matter Search Results from a One Ton-Year Exposure of XENON1T*, *Phys. Rev. Lett.* **121** (2018) 111302 [arXiv:1805.12562] [INSPIRE].

[57] M. Klasen, C.E. Yaguna and J.D. Ruiz-Alvarez, *Electroweak corrections to the direct detection cross section of inert Higgs dark matter*, *Phys. Rev.* **D 87** (2013) 075025 [arXiv:1302.1657] [INSPIRE].

[58] ICECUBE collaboration, *Search for annihilating dark matter in the Sun with 3 years of IceCube data*, *Eur. Phys. J.* **C 77** (2017) 146 [*Erratum ibid.* **C 79** (2019) 214] [arXiv:1612.05949] [INSPIRE].

[59] MAGIC and FERMI-LAT collaborations, *Limits to Dark Matter Annihilation Cross-Section from a Combined Analysis of MAGIC and Fermi-LAT Observations of Dwarf Satellite Galaxies*, *JCAP* **02** (2016) 039 [arXiv:1601.06590] [INSPIRE].

[60] D. Eriksson, J. Rathsman and O. Stal, *2HDMC: Two-Higgs-Doublet Model Calculator Physics and Manual*, *Comput. Phys. Commun.* **181** (2010) 189 [arXiv:0902.0851] [INSPIRE].

[61] D. Barducci et al., *Collider limits on new physics within MicrOMEGAs_4.3*, *Comput. Phys. Commun.* **222** (2018) 327 [arXiv:1606.03834] [INSPIRE].

JHEP07(2019)053

[62] B. Dutta, G. Palacio, J.D. Ruiz-Alvarez and D. Restrepo, *Vector Boson Fusion in the Inert Doublet Model*, *Phys. Rev.* **D 97** (2018) 055045 [arXiv:1709.09796] [INSPIRE].

[63] CMS collaboration, *Search for invisible decays of a Higgs boson produced through vector boson fusion in proton-proton collisions at* $\sqrt{s} = 13$ *TeV*, *Phys. Lett.* **B 793** (2019) 520 [arXiv:1809.05937] [INSPIRE].

[64] J. Kalinowski, W. Kotlarski, T. Robens, D. Sokolowska and A.F. Żarnecki, *IDM benchmarks for the LHC at 13 and 27 TeV*, Submitted to the Higgs Cross Section Working Group, October 2018.

[65] T. Robens, *IDM benchmarks for the LHC at 13 and 27 TeV*, talk at *The Higgs Cross Section Working Group Wg3 Subgroup Meeting*, 24 October 2018 [https://indico.cern.ch/event/767041/].

[66] F. Zimmermann et al., *Future Circular Collider*, CERN-ACC-2018-0059.

[67] M. Moretti, T. Ohl and J. Reuter, *O'Mega: An Optimizing matrix element generator*, hep-ph/0102195 [INSPIRE].

[68] W. Kilian, T. Ohl and J. Reuter, *WHIZARD: Simulating Multi-Particle Processes at LHC and ILC*, *Eur. Phys. J.* **C 71** (2011) 1742 [arXiv:0708.4233] [INSPIRE].

[69] F. Staub, *Exploring new models in all detail with SARAH*, *Adv. High Energy Phys.* **2015** (2015) 840780 [arXiv:1503.04200] [INSPIRE].

[70] W. Porod, *SPheno, a program for calculating supersymmetric spectra, SUSY particle decays and SUSY particle production at* e^+e^- *colliders*, *Comput. Phys. Commun.* **153** (2003) 275 [hep-ph/0301101] [INSPIRE].

[71] W. Porod and F. Staub, *SPheno 3.1: Extensions including flavour, CP-phases and models beyond the MSSM*, *Comput. Phys. Commun.* **183** (2012) 2458 [arXiv:1104.1573] [INSPIRE].

[72] L. Linssen, A. Miyamoto, M. Stanitzki and H. Weerts, *Physics and Detectors at CLIC: CLIC Conceptual Design Report*, arXiv:1202.5940 [INSPIRE].

[73] A. Hocker et al., *TMVA — Toolkit for Multivariate Data Analysis*, physics/0703039 [INSPIRE].

[74] A. Robson and P. Roloff, *Updated CLIC luminosity staging baseline and Higgs coupling prospects*, arXiv:1812.01644 [INSPIRE].

JHEP07(2019)053